Nuclear Engineering and Design 337 (2018) 460–470

Contents lists available at ScienceDirect

Nuclear Engineering and Design

journal homepage: www.elsevier.com/locate/nucengdes

CANDU-6 reactivity devices optimization for advanced cycles – Part II: Liquid zone controllers adjustment

Emmanuel St-Aubin*, Guy Marleau

Institut de Génie Nucléaire, École Polytechnique de Montréal, P.O. Box 6079, Station Centre-Ville, Montréal, Québec, Canada H3C 3A7

ARTICLE INFO

Keywords:
Reactivity devices
CANDU
Thorium
Fuel management
DONJON

ABSTRACT

In Part I of this paper, we optimized the CANDU-6 adjuster rods for reactors burning thorium-based fuel. Here we modify the liquid zone controllers assuming optimized adjuster rods for the same advanced cycles. The objective is to maximize the average exit burnup for these fuel cycles while preserving the reactor ability to control the power distribution inside the core during normal operation conditions. These goals are achieved by implementing a liquid zone controller iterative response model based on explicit diffusion calculations to evaluate the control system capacity to maintain zone, channel and bundle powers below their safety limits during predetermined perturbations sequences. Based on the evaluation of spatial control metrics for on-power refueling, boric acid or heavy water doping of the light water in the controllers is selected. A full core model is also used to assess their response during adjuster rods withdrawal in shim mode. The results demonstrate that our approach works well for thorium-based cycles, while achieving excellent fuel management performances. The use of D_2O-doped liquid zone controllers for the natural uranium cycle can also increase its average exit burnup by 0.7% without detrimental consequences on reactor control.

1. Introduction

The CANDU-6 reactor regulating system (RRS) controls four types of reactivity systems (Rouben, 1984), the two most important being the adjuster rods (ADJ) and the liquid zone controllers (LZC) since they are normally inserted in the reactor and used at full power. The adjuster rods are mainly used to flatten the flux distribution in the core and to provide a positive reactivity reserve that can be used when required. Liquid zone controllers provide fine reactivity adjustments and spatial power control capabilities. The other two systems are the mechanical control absorbers (MCA) that can be inserted from the top of the core to decrease rapidly the core power and a set of valves to inject boric acid solution in the moderator to compensate the large excess reactivity of the fresh core.

In the first part of this paper (St-Aubin and Marleau, 2015b), we optimized the adjuster rods to preserve the reference operational requirements of natural uranium (NU) fuel for reactor trip and shim mode operation regimes for advanced fuel cycles. To achieve our adjusters performance objectives while maximizing the economical advantages of the cycles, we selected an algorithm combining geometrical modification and rods material doping coupled with a fuel management optimization method (St-Aubin and Marleau, 2015a). These studies were performed for selected thorium-based cycles driven by LEU or DUPIC (Direct Use of PWR spent fuel In CANDU) fuels.

Supercell calculations indicate that the static reactivity worth of the nominal LZC decreases by up to 17% for these thorium-based fuels when compared with the reference (St-Aubin and Marleau, 2012; St-Aubin and Marleau, 2015c; St-Aubin, 2013). The use of a 4-bundle shift refueling pattern in advanced cycles induces a depression in the axial flux shape at the core center not observed with the reference 8-bundle shift strategy. The liquid zone controllers should therefore be modified to meet the CANDU safety requirements.

LZC response during on-power refueling in natural uranium and DUPIC cycles were evaluated by many authors (Rozon et al., 1997; Choi, 2000; Jeong and Choi, 2000; Choi and Kim, 2005; Do et al., 2006). However, these studies never considered modifying the liquid zone controllers to enhance their capacity to manage the power distribution during normal operations in advanced cycles. Here, we propose to adjust the LZC for thorium cycles, the objective being to ensure that their performance is similar to what is observed for the NU fuel cycle. We assume that their geometry and locations in the core cannot be modified. This is partly justified by the computational challenge of generating accurate LZC incremental cross sections (St-Aubin and Marleau, 2015c). The only way to change their reactivity worth is then by doping the light water that fills the various sections of a LZC using different materials.

* Corresponding author.
E-mail addresses: emmanuel.st-aubin@polymtl.ca (E. St-Aubin), guy.marleau@polymtl.ca (G. Marleau).

https://doi.org/10.1016/j.nucengdes.2018.06.026
Received 6 March 2017; Received in revised form 16 June 2018; Accepted 26 June 2018
Available online 01 August 2018

List of acronyms

ADJ	adjuster rods
CANDU	Canada deuterium uranium
CANFLEX	CANDU flexible
DUPIC	Direct Use of PWR spent fuel In CANDU
E	optimal time-average equilibrium state
F	fresh core state
FPD	full power days
LEU	low-enriched uranium
LZC	liquid zone controllers
MCA	mechanical control absorbers
NEE	natural equivalent enrichment
NU	natural uranium
PWR	pressurized water reactor
R	refueled core state
RRS	reactor regulating system
TD	thorium-DUPIC cycle
TU	thorium-uranium cycle

In Section 2, we briefly recapitulate the modeling of the CANDU-6 and describe in details the roles, requirements and nominal performances of the LZC system. In Section 3, we propose a response model that will be used by our LZC modification strategy to assess their capacity to manage power tilts during normal operation. In Section 4, the light water doping strategy is analyzed in details, a method to generate credible core perturbations in normal operation is provided and the operational constraints used in the simulations are discussed. Section 5 provides a detailed analysis of the reference cycle during perturbations sequences, as well as our LZC optimal doping selection process applied to three different fuel cycles. Finally, the main conclusions of this study are highlighted and perspectives for future work are discussed in Section 6.

2. Reactor model and liquid zone controllers system

As described extensively in St-Aubin and Marleau (2015a), the reactivity and the power distribution in a CANDU is generally obtained by solving the diffusion equation using 2-group burnup-dependent cross sections $\Sigma^G(\mathscr{B})$ and diffusion coefficients $D^G(\mathscr{B})$ derived from 2D and 3D multigroup transport calculations. The incremental macroscopic cross sections databases for the LZC (and the other devices) are generated at static burnup $\mathscr{B}_S$ using an accelerated pseudo-exact 3D supercell model (St-Aubin and Marleau, 2015c). The reference average thermal field in the core, constant pressures, densities and isotopic purities for both the coolant and moderator are considered in all transport calculations. Local parameters effects are neglected.

The liquid zone controllers have the most complex geometry of all CANDU devices. They are distributed on two identical *XY* planes in the reactor, each having three vertical controllers. The controllers are divided vertically (direction *Y*) into two or three compartments partly filled of light water. The upper part of the compartment is filled with helium gas to measure the light water level. LZC are crossed from the bottom to the top by two types of tubes, each being subdivided radially into two concentric regions. Small scavenger/bubbler and large feeder/balance (external/internal region) tubes are always filled with helium (internal) and light water (external). With this underlying system, each LZC compartment can be filled or emptied independently. Fig. 1 illustrates the location of LZC in the core *XZ* plane while Fig. 2 presents the LZC configuration in the *XY* plane along with the three LZC section types. Fig. 3 illustrates the geometry of LZC32, LZC21 and LZC10, where the two integers refer respectively to the number of scavenger/bubbler and feeder/balance tubes in the compartment.

It is worth noting that if one attempts to adjust LZC capability by modifying them geometrically, as we did for the ADJ, the fluids injection systems, as well as the couplings between the compartments of a given rod, might have to be re-designed.

The main role of the LZC is to control reactivity decreases between refuelings for normal operation and increases after adjuster banks withdrawal during shim mode regime. They are also used to maintain the power distribution in the core below safety limits and close to the ideal designed distribution during refueling at full power. In fact, the equilibrium CANDU-6 core fueled with natural uranium is designed to be critical with all the LZC compartments half-filled with light water. Tuning finely the filling level of the respective compartments allows to control the local power distribution in the core.

The reactor regulating system adjusts the water level in a LZC compartment based on the signal from two types of detectors: 28 platinum detectors distributed over 14 control zones (2 detectors/zone) in the core; and ion chambers located outside the core. They measure respectively the control zone powers $\mathscr{P}_c(t)$ and the total core power $\mathscr{P}(t)$ at time *t*. Note that when the total core power reaches 5% above its set point, the regulation is ensured by the platinum detectors. The Flux Mapping System recalibrates these detectors at 2 minutes intervals. Seven control zones cover each axial half of the core (see Fig. 2). The water level $\mathscr{Y}_c(t)$ (measured in filling percentage) for the compartment located in control zone *c* is adjusted in such a way as to achieve zonal and total power set points ensuring core integrity and design power distribution at all time. Thus, detector signals indicating local power deviations from the set points will lead to the activation of the valves controlling the water level of the LZC. This will continue until a new equilibrium is reached. This equilibrium depends on the power set points and initial filling fractions of the LZC. In practice, compartments with $\mathscr{Y}_c(t) \leqslant 10\%$ or $\mathscr{Y}_c(t) \geqslant 80\%$ are less solicited than the others for the control of the total core power (Varin et al., 1995), but here we neglect this nonlinearity of the LZC response. In this study, we also assume that the LZC response is instantaneous.

Even if in practice the RRS changes LZC water levels independently, their capacity to influence the flux distribution is related to their total

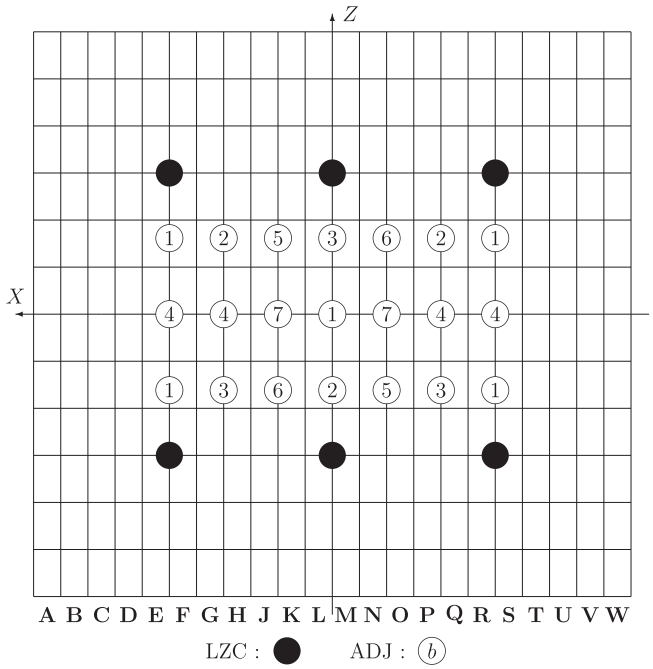

Fig. 1. LZC and adjuster banks (b = 1, 7) configuration in the core *XZ* plane. The rectangular fuel bundles are 49.53 cm long and 28.575 cm wide.

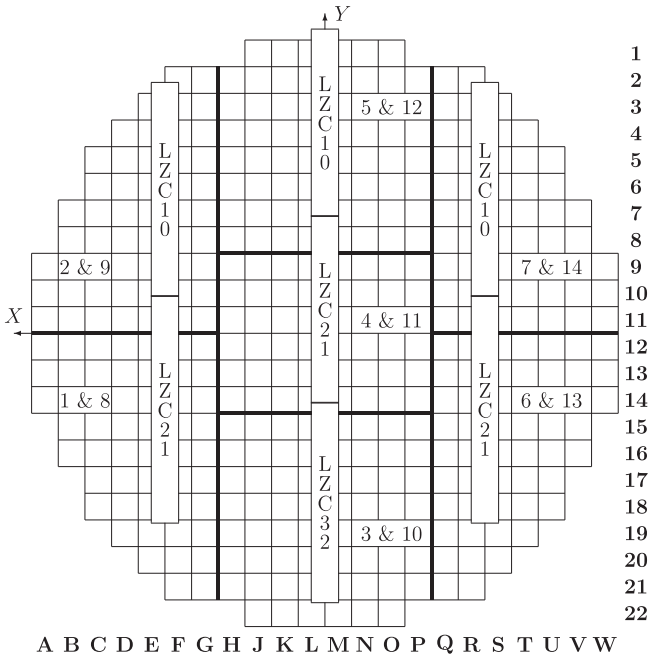

Fig. 2. Liquid zone controllers configuration in the *XY* plane with the LZC section types, control zones limits (thick lines) and numbering. The white squares represent fuel channels with a lattice pitch of 28.575 cm.

reactivity worth ρ_{LZC}. Assuming the LZC are either 0%, 50% or 100% filled with all adjuster rods inserted in the core, the total LZC reactivity worth

$$\rho_{LZC} = \rho_{\downarrow} - \rho_{\uparrow} = 10^5 \text{pcm} \times \left(\frac{1}{k_{\text{eff}}^{100\%}} - \frac{1}{k_{\text{eff}}^{0\%}} \right), \tag{1}$$

where

$$\rho_{\uparrow} = 10^5 \text{pcm} \times \left(\frac{1}{k_{\text{eff}}^{50\%}} - \frac{1}{k_{\text{eff}}^{100\%}} \right) \tag{2}$$

$$\rho_{\downarrow} = 10^5 \text{pcm} \times \left(\frac{1}{k_{\text{eff}}^{50\%}} - \frac{1}{k_{\text{eff}}^{0\%}} \right) \tag{3}$$

are reactivity changes that result from filling from 50% to 100% or emptying from 50% to 0% all LZC, respectively.

Table 1 presents $\rho_{\downarrow}$, $\rho_{\uparrow}$ and ρ_{LZC} for the three different cycles studied in St-Aubin and Marleau (2015a):

- NU, the reference natural uranium fuel placed in a 37-element fuel bundle;
- TU, an homogeneous fuel that contains 60 v.% of ThO_2 and 40 v.% of 5.0 wt.% enriched UO_2 placed in a CANFLEX 43-element fuel bundle; and
- TD, an heterogeneous 37-element fuel bundle with the 7 central pins filled with ThO_2 (18.9 v.%) and the outer 30 pins filled with DUPIC dioxide (81.1 v.%). The DUPIC composition considered here is described in Choi et al. (1997).

Table 1
LZC reactivity worth for NU, TU and TD cycles in E, F and R states (pcm).

Cycles	NU			TU			TD		
States	E	F	R	E	F	R	E	F	R
$\rho_{\uparrow}$	−332	−301	−304	−221	−311	−311	−208	−318	−315
$\rho_{\downarrow}$	421	395	397	276	395	393	274	416	416
ρ_{LZC}	753	695	701	497	706	704	482	734	730

Both the optimal equilibrium (E), fresh core (F) and refueled core (R) states were considered (St-Aubin and Marleau, 2015a). We observe that

$$|\rho_{\downarrow}/\rho_{\uparrow}| < 1$$

for all cases, since the local flux level seen by the LZC is higher after they are emptied than when they were filled. Moving from the equilibrium to an instantaneous state strongly increases ρ_{LZC} for TU and TD fuels. This is because both cycles use a 4-bundle shift refueling strategy that results in an axial flux shape that is more peaked in the planes $k = 3, 4, 9, 10$ where the LZC are located. For the NU cycle with 8-bundle shift, ρ_{LZC} is lower for the fresh than the equilibrium core because the axial flux shape is less peaked at these positions while for the refueled core, the decrease in reactivity is due to the higher average fuel age near the LZC than at equilibrium.

3. Liquid zone controllers response modeling

The LZC response to perturbations in the core power distribution is controlled by the RRS. The LZC system reacts to two types of external interventions by the operators: 1) channel refueling in normal operation, and 2) withdrawal of the adjuster rod banks during shim mode operation. In addition, the RRS also adjusts the LZC constantly to compensate reactivity loss due to fuel burnup. Accordingly, designing a simplified RRS that simulates adequately the behavior of the LZC is not a trivial task. It must be able to deal with the large perturbations resulting from operator interventions and to re-equilibrate the power distribution in the core in such a way that no power limits are ever exceeded. To achieve this goal, we propose to use an iterative constrained optimization technique based on explicit diffusion calculations coupled in a coherent manner with a full core quasi-static fuel evolution method. Here, we first discuss the basic behavior of the RRS and introduce our quasi-static core reactivity model. Then, the LZC response model is presented before describing our simplified simulation algorithm.

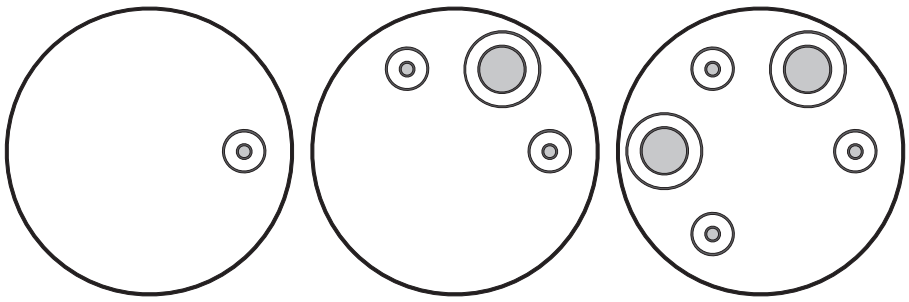

Fig. 3. Liquid zone controllers LZC10 (left), LZC21 (center) and LZC32 (right) geometries.

3.1. Simplified RRS and quasi-static core reactivity models

We first assume that the shutdown system can be totally ignored since it will not be activated in our simulations. We also exclude the MCA from our model although they can be inserted in the core as soon as the LZC average filling level

$$\langle \mathscr{Y}(t) \rangle = \frac{1}{14} \sum_{c=1}^{14} \mathscr{Y}_c(t) \tag{4}$$

exceeds 80% or the total reactor power exceeds its set point by 1.5% (Varin, 1995). With our reactor model (see Section 2), the core static reactivity variation during operation, $\delta\rho(t)$, can be decomposed into four components as

$$\delta\rho(t) = \delta\rho_{\text{refuel}}(t) + \delta\rho_{\text{burn}}(t) + \delta\rho_{\text{ADJ}}(t) + \delta\rho_{\text{LZC}}(t). \tag{5}$$

$\delta\rho_{\text{refuel}}(t)$ is the reactivity insertion in the core due to refueling and $\delta\rho_{\text{burn}}(t)$ the reactivity loss from burnup. For shim mode operation, $\delta\rho_{\text{ADJ}}(t)$ represents the reactivity insertions resulting from adjuster banks withdrawal, while $\delta\rho_{\text{ADJ}}(t) = 0$ during normal operation. Finally, $\delta\rho_{\text{LZC}}(t)$ is the total reactivity change resulting from LZC level variations. In St-Aubin (2013), we also consider other core modeling effects that we do not analyze here.

For this study, an adjuster bank b (see Fig. 1) is either considered totally inserted ($\mathscr{Y}_b(t) = 100\%$) or extracted ($\mathscr{Y}_b(t) = 0\%$) from the core and its motion is assumed to be instantaneous at the time t_b when it is extracted. As a result, we have

$$\delta\rho_{\text{ADJ}}(t) = \sum_{b=1}^{7} \rho_b(t) H(t-t_b) \tag{6}$$

with $\rho_b(t) > 0$ the reactivity worth of reactivity bank b at time t and $H(t-t_b)$ the Heaviside function defined as

$$H(t) = \begin{cases} 0, & t < 0 \\ 1, & t \geq 0 \end{cases}.$$

The time t_b at which the bank b is extracted from the core is defined with the actual ADJ driving rules:

$$\langle \mathscr{Y}(t_b) \rangle = 20\%, \tag{7}$$

i.e. the moment when the average LZC level $\langle \mathscr{Y}(t) \rangle$ decreases to 20%.

When a bank is extracted from the core, $\langle \mathscr{Y}(t) \rangle$ increases to keep the core critical, providing shim mode operation time before the next bank withdrawal ($t_b \geq t_{b-1}$) if one of the fueling machines is unavailable. Otherwise, the operator refuels the next channel j in the fueling sequence inserting reactivity in the core. The variation in core static reactivity due to refuelings with time t is given by

$$\delta\rho_{\text{refuel}}(t) = \sum_{j} \rho_j(t) H(t-t_j), \tag{8}$$

where $\rho_j(t)$ is the reactivity gain provided by the refueling of channel j at time t_j.

The RRS system reacts to these operator actions by adjusting the individual LZC water levels to make the core critical and to satisfy zonal power constraints. The natural way to conceive this dynamic is to consider that the former objective is achieved by varying the LZC average filling level $\langle \mathscr{Y}(t) \rangle$, while the latter is attained by setting the individual LZC water level deviations from the average $\mathscr{Y}_c(t) - \langle \mathscr{Y}(t) \rangle$ properly. Here, we adopt a more convenient but slightly different view that consists in decomposing the LZC levels into a global $\mathscr{Y}_G(t)$ component, common to all compartments, and a spatial component $\delta\mathscr{Y}_c(t)$, that is compartment-dependent:

$$\mathscr{Y}_c(t) = \mathscr{Y}_G(t) + \delta\mathscr{Y}_c(t). \tag{9}$$

Considering $\partial\delta\rho_{\text{LZC}}(t)/\partial\mathscr{Y}_c$ as the quasi-static reactivity coefficients of the individual LZC water levels $\mathscr{Y}_c(t)$, we can write:

$$\frac{\partial\delta\rho_{\text{LZC}}(t)}{\partial t} = \sum_{c=1}^{14} \frac{\partial\delta\rho_{\text{LZC}}(t)}{\partial\mathscr{Y}_c} \left[\frac{\partial\mathscr{Y}_G(t)}{\partial t} + \frac{\partial\delta\mathscr{Y}_c(t)}{\partial t} \right], \tag{10}$$

with

$$\frac{\partial\mathscr{Y}_G(t)}{\partial t} = \sum_r \Delta\mathscr{Y}_G(t)\delta(t-t_r), \tag{11}$$

$$\frac{\partial\delta\mathscr{Y}_c(t)}{\partial t} = \sum_r \Delta\mathscr{Y}_c(t)\delta(t-t_r), \tag{12}$$

where $\sum_r .\delta(t-t_r)$ is the Dirac comb operator over the instants t_r when the LZC responses take place, whereas $\Delta\mathscr{Y}_G(t) = \mathscr{Y}_G(t^+) - \mathscr{Y}_G(t^-)$ and $\Delta\mathscr{Y}_c(t) = \delta\mathscr{Y}_c(t^+) - \delta\mathscr{Y}_c(t^-)$ are respectively the global and spatial LZC response amplitudes at time t. Here $t^\pm = t \pm \delta t$ are the times just before and after t, with $\delta t > 0$ being a small quantity.

Once the power distribution is controlled after refueling or adjuster bank withdrawal, fuel burnup can proceed in credible conditions. Each bundle in the core is then burned for a sequence of time steps $\Delta t_r = t_{r+1} - t_r$ sufficiently small to consider their power constant between two successive LZC response times (i.e. for $t \in [t_r^+, t_{r+1}^-]$). It is crucial to note that response times t_r (and associated time steps Δt_r) is not imposed *a priori*. It is determined dynamically by the simulation algorithm with regard to the current reactor behavior in order to respect a set of RRS modeling constraints described in the following and the assumption that the power remains nearly constant over Δt_r. The burnup distribution in the core at time t_{r+1} is given by

$$\mathscr{B}_{jk}(t_{r+1}) = \mathscr{B}_{jk}(t_r) + \frac{\mathscr{P}_{jk}(t_r^+)\Delta t_r}{m_{\text{he}}}, \tag{13}$$

where m_{he} is the initial mass of heavy elements in the fuel bundle and $\mathscr{P}_{jk}(t_r^+)$ is the power produced by bundle k in channel j at time t_r^+, i.e. immediately after the re-assessment of the power distribution (diffusion calculation) at $t = t_r$. This distinction is important since $\mathscr{B}_{jk}(t_r^-) = \mathscr{B}_{jk}(t_r^+)$, but $\mathscr{P}_{jk}(t_r^-) \neq \mathscr{P}_{jk}(t_r^+)$. The quasi-static fuel evolution stops at time $t = t_{r_{\max}}$, which depends on the perturbations sequences and LZC light water doping level (see Section 4).

With this RRS model, the core state at time t is totally determined by $\mathscr{P}(t)$, $\mathscr{B}_{jk}(t)$, $\mathscr{Y}_b(t)$ and $\mathscr{Y}_c(t)$. Our LZC response model consists in determining the global and spatial LZC response amplitudes $\Delta\mathscr{Y}_G(t)$ and $\Delta\mathscr{Y}_c(t)$ in Eqs. (11) and (12) in such a way as to cancel Eq. (5) by taking explicitly into account local instantaneous quasi-static reactivity coefficients $\partial\delta\rho_{\text{LZC}}(t)/\partial\mathscr{Y}_c$ at a response time $t = t_r$. Those, along with the power distribution $\mathscr{P}_{jk}(t)$, are evaluated by diffusion calculations. This determines stationary LZC water levels $\mathscr{Y}_c(t_r^+)$ after a given perturbation varying $\delta\rho_{\text{ADJ}}(t)$ (via $\mathscr{Y}_b(t)$) or $\delta\rho_{\text{refuel}}(t)$ (see Section 4.2). The LZC response model is implemented in 2 coupled iterative levels. First, the global iteration computes $\Delta\mathscr{Y}_G(t)$ required to reach criticality ensuring that the total power $\mathscr{P}(t)$ keeps its set point at time t. Then, the spatial iteration evaluates $\Delta\mathscr{Y}_c(t)$ to maintain the shape of the power distribution under the prescribed safety limits. Finally, this model is coupled with a quasi-static fuel evolution model, that follows the burnup distribution $\mathscr{B}_{jk}(t)$ in time, to quantify the effects on core reactivity $\delta\rho_{\text{burn}}(t)$.

3.2. Quasi-static LZC response and fuel evolution models

The LZC response algorithm we propose is controlled externally by two types of operator actions: refuelings during normal operation and adjuster banks withdrawal during shim mode operation. Two embedded iteration processes deal respectively with spatial (outer iteration) and global (inner iteration) LZC level components adjustment, whereas appropriate time steps Δt_r for the quasi-static fuel evolution are selected in a coherent manner with our simplified RRS model.

3.2.1. Global iteration

The objective of the global (inner) iteration is to bring the core back

to criticality after any perturbation. Since the ion chambers measuring the total reactor power have a certain sensitivity below which the measurements can be considered as noise, perturbations in reactivity smaller in absolute value than a certain threshold $\rho_0 > 0$ are considered irrelevant. In such cases, no action from the LZC is required. Otherwise, a request is sent to the control valves to vary uniformly the LZC filling levels (via $\mathscr{Y}_G(t)$) in such a way that the reactor becomes very slightly supercritical

$$\rho[\mathscr{Y}_G(t_r^+)] = \rho_0. \tag{14}$$

We then use the Brent's method (Brent, 1973) to solve this nonlinear problem. A numerical tolerance $\varepsilon > 0$, a maximal number of iteration $l^{\max}$, and two bounds $\mathscr{Y}_G^{\pm}$ such that

$$(\rho[\mathscr{Y}_G^+]-\rho_0) \times (\rho[\mathscr{Y}_G^-]-\rho_0) < 0,$$

are required to start and control this algorithm. The natural choices are $\mathscr{Y}_G^- = 0\%$ and $\mathscr{Y}_G^+ = 100\%$. A special condition in the algorithm ensures that this implies $\mathscr{Y}_c(t) = 0\%$ and $\mathscr{Y}_c(t) = 100\%$ respectively, even if $\delta\mathscr{Y}_c(t) \neq 0\%$. If after $l_G^{\max}$ iterations one still have

$$|\rho[\mathscr{Y}_G(t_r^+)]| > \rho_0 + \varepsilon$$

then the total LZC reactivity worth is insufficient to control the reactor and the LZC are not adequate for the cycle considered. The algorithm then stops. Otherwise, this procedure determines $\Delta\mathscr{Y}_G(t_r)$ of Eq. (11) at $t = t_r$ for fixed spatial components. Note that once $\mathscr{Y}_G(t_r^+)$ is determined with Eq. (14), the $\delta\mathscr{Y}_c(t)$ for some compartments may have to be corrected in such a way as to maintain $\mathscr{Y}_c(t)$ between 0% and 100%.

3.2.2. Spatial iteration

Once the global LZC component is determined (ρ in the range $]\rho_0-\varepsilon, \rho_0 + \varepsilon[$), the shape of the power distribution is readjusted. Denoting the spatial component of the LZC filling fraction in control zone c at the beginning of the m-th spatial (outer) iteration performed at time $t = t_r$ by $\Delta\mathscr{Y}_c^{(m)}(t_r)$, then the LZC levels will be corrected using

$$\Delta\mathscr{Y}_c^{(m+1)}(t_r) = \Delta\mathscr{Y}_c^{(m)}(t_r) + \Delta\widetilde{\mathscr{Y}} \times [\mathscr{H}_j^{(m)}(t_r) + \mathscr{H}_{jk}^{(m)}(t_r) + \mathscr{H}_c^{(m)}(t_r)], \tag{15}$$

where

$$\mathscr{H}_x(t) = \begin{cases} 0, & \text{if } \mathscr{P}_x^{\max}(t^-) < \mathscr{P}_x^{\lim}(t^-) \\ 1, & \text{otherwise} \end{cases} \tag{16}$$

with $x \in \{jk, j, c\}$. The use of the superscript (m) on $\mathscr{H}_x(t)$ means that $\mathscr{P}_x^{\max}(t^-) = \mathscr{P}_x^{\max,(m)}(t^-)$ in Eq. (16). At any iteration m, the channel component $\mathscr{H}_j^{(m)}(t_r) = 1$ only in the 2 control zones c (core front-end) and $c + 7$ (core back-end) where the channel with the maximal power $\mathscr{P}_j^{\max,(m)}(t_r^-)$ is located. Similarly, the bundle component $\mathscr{H}_{jk}^{(m)}(t_r)$ is unity only in the control zone where the maximal bundle power $\mathscr{P}_{jk}^{\max,(m)}(t_r^-)$ is observed. Finally, the control zone component $\mathscr{H}_c^{(m)}(t_r)$ is set to 1 in every zones where the zone power $\mathscr{P}_c^{(m)}(t_r^-)$ exceeds the zone power limit $\mathscr{P}_c^{\lim}(t_r^-)$. The power limits are given explicitly in Section 4.3. This results in step increases of 0, $\Delta\widetilde{\mathscr{Y}}$, $2\Delta\widetilde{\mathscr{Y}}$ or $3\Delta\widetilde{\mathscr{Y}}$ depending on the total number of power limits types (channel, bundle or zone) exceeded in control zone c. Here, the parameter $\Delta\widetilde{\mathscr{Y}} > 0$ represents the maximal numerical uncertainty allowed on the LZC spatial response amplitudes $\Delta\mathscr{Y}_c(t_r)$.

The outer iteration stops if $\Delta\mathscr{Y}_c^{(m+1)}(t_r) = \Delta\mathscr{Y}_c^{(m)}(t_r)$, i.e. when all power constraints are satisfied ($\mathscr{H}_x^{(m)}(t_r) = 0, \forall\, x$) or if the maximal number of iterations $m^{\max}$ is reached. Note that it is important to set $\Delta\widetilde{\mathscr{Y}}$ and $m^{\max}$ in such a way that $\Delta\widetilde{\mathscr{Y}} \times m^{\max} \geqslant 100\%$ in order to let the LZC filling levels vary over their whole range and avoid reducing artificially their potential to control the shape of the power distribution. When convergence is reached, the global iteration is activated again to return the core with converged LZC spatial components to criticality via the LZC global component.

This global-spatial coupled iteration process is repeated until convergence is reached after a single outer iteration, leading to $\Delta\mathscr{Y}_c(t_r) = 0$ and the sought after stationary LZC water levels $\mathscr{Y}_c(t_r^+)$. A maximal number of coupled global-spatial iterations $n^{\max}$ is also imposed. Finally, when global-spatial convergence is reached, one can then proceed with the quasi-static fuel evolution before considering another LZC response.

3.2.3. Fuel burnup

Once the core reactivity and power distribution are controlled, fuel burnup can proceed in credible conditions. Then, one has to select the width $\Delta t_r = t_{r+1}^- - t_r^+$ of the next time step. For normal reactor operation, one option could be to select $\Delta t = 1/\overline{\mathscr{F}}$ for all time steps, where $\overline{\mathscr{F}}$ is the time-average refueling frequency (see Section 4.2.2). However, this is equivalent to deactivating the RRS during the burnup period, which is the opposite of what we want to do.

When the global-spatial iterative process has converged, the reactor is still slightly supercritical with $\rho(t_r^+) \in]\rho_0-\varepsilon, \rho_0 + \varepsilon[$, corresponding to the upper bound of the detector sensitivity interval (see Section 3.2.1). Moreover, for a critical core, a perturbation in reactivity of at least ρ_0 (plus numerical tolerance effects) is required to activate the RRS system. Since burnup reduces the reactivity for a core at equilibrium, the minimal time interval for burnup corresponds to a reduction of the reactivity by $2\rho_0$, which leads to a core almost critical when the reactivity is averaged over time and the perturbations effects are neglected. Accordingly, Δt_r should be selected in such a way that

$$\rho(t_r^+ + \Delta t_r) = -\rho_0, \tag{17}$$

which corresponds to the lower bound of the detector sensitivity interval. This problem is solved again with Brent's method with a tolerance $\varepsilon > 0$. One of the bound is $\Delta t_r = 0$ corresponding to $\rho(t_r^+) > 0$ and the second bound $\Delta t_{\max} > \rho_0/(\partial\delta\rho(t)/\partial t)$ corresponds to $\rho(t_r^+ + \Delta t_{\max}) < -\rho_0$. Here, we set $\Delta t_{\max} = 4$ FPD, which is sufficiently high for all the cycles we have tested (St-Aubin, 2013).

Thus, the time of the next LZC response t_{r+1} corresponds to the next moment $t > t_r$ at which, according to the adopted RRS control rules, the reactivity crosses the lower or the upper bound of the detector sensitivity interval due to fuel burnup or an external core perturbation (refueling of a channel or the withdrawal of an adjuster rods bank), respectively. Finally, if Δt_r is such that

$$t_r + \Delta t_r > t_{r_{\max}}$$

then the burnup step will be reduced to $\Delta t_r = t_{r_{\max}} - t_r$ to match the duration of the perturbation sequences.

4. Core perturbations and optimization constraints

In this section we first analyze the consequences of doping the light water in the LZC on the optimal equilibrium core state of the advanced cycles considered here (see Section 2). We then present two perturbations sequences that allow to assess the capacity of the modified LZC to control the core reactivity and power distribution when coupled with the LZC response and fuel evolution models presented in Section 3.2. Finally, we make some remarks on the implementation of the algorithm and discuss in details the optimization constraints selected with regards to core perturbations.

4.1. Doping of the light water

Although LZC requirements are only indirectly related to their reactivity worth (see Section 2), the LZC modification strategy can still be based on their neutron absorption capability that controls ρ_{LZC}. As discussed before, we decided to keep their geometry and underlying systems unchanged and to consider only the possibility of doping the light water to modify the LZC. Two options can then be selected: increasing and decreasing the LZC absorption rate using nuclei more or less absorbing than the hydrogen present in light water.

A boric acid solution diluted in the LZC light water circuitry can be used to increase ρ_{LZC}. H_3BO_3 has a molar mass of 61.833 g/mol, a density of 1.435 g/cm^3 at 15°C, a maximum solubility in water of 47.2 g/L at 20°C, contains 17.48 wt.% of natural boron (19.9 at.% of ^{10}B and 80.1 at.% of ^{11}B) (Harper et al., 2012). It is currently used for moderator poisoning in PWR and CANDU, since $\sigma_{\alpha,^{10}B} = 3.84$ kb is large when compared with $\sigma_{\gamma,^1H} = 333$ mb and $\sigma_{\gamma,^2H} = 506\ \mu$b for 0.025 eV neutrons (Shultis and Faw, 2008). Note that boric acid concentration in light water $c_{H_3BO_3}$ must remain under a certain threshold to avoid excessive corrosion, precipitation or explosive H_2O_2 production by radiolysis. Here, we limit $c_{H_3BO_3}$ to 2500 ppm, which is similar to typical concentrations found in PWR (Reuss, 2003). This limit is huge when compared with what is usually injected in CANDU moderator during the early core period (typically around 7 ppm at $t = 0$) (Rouben, 1984; St-Aubin and Marleau, 2015a), but the LZC volume is very small when compared with the reactor vessel.

If the goal is to decrease ρ_{LZC}, it is possible to mix heavy water with H_2O. The D_2O volume fraction in light water v_{D_2O} is limited to 90 v.% since simulations have shown that for $v_{D_2O} > 90$ v.% (D_2O purity is 99.92 v.% in the moderator), filling the LZC leads to an increase in core reactivity. This is the opposite of the expected and desired behavior and is due to an increase in neutrons slowing down efficiency in D_2O-doped LZC, thus increasing the fission rate in the fuel.

To simplify the notation, we define the normalized LZC doping

$$c_{LZC} = \begin{cases} -\frac{v_{D_2O}}{1\text{v.\%}}, & \text{for heavy water doping} \\ 0, & \text{without doping} \\ \frac{c_{H_3BO_3}}{25\text{ppm}}, & \text{for boric acid doping,} \end{cases} \tag{18}$$

in such a way that $c_{LZC} \in [-90, 100]$. Fig. 4 presents ρ_{LZC} computed at the optimal equilibrium (state E) as a function of c_{LZC} for NU, TU and TD cycles. Note that 2 supercell calculations ("IN" and "OUT" states, see St-Aubin and Marleau (2015a)) are required for every points of these curves which have similar shapes. For $c_{LZC} < 0$, considering that it is H_2O that dopes D_2O in a proportion varying like 100v. %$-v_{D_2O}$, a mild saturation of ρ_{LZC} is observed as c_{LZC} increases toward 0. For $c_{LZC} > 0$, the saturation is more marked as expected since $\sigma_{a,^{nat}B} - \sigma_{a,^1H} \gg \sigma_{a,^1H} - \sigma_{a,^2H}$ and that the flux level decreases locally near H_3BO_3-doped LZC. The doping efficiency $\rho_{LZC}(c_{LZC})/\rho_{LZC}(0)$ is lower for the NU cycle than for TU and TD cycles, since a lower $\rho_{LZC}(0)$ (see Table 1) means a higher sensitivity to changes in the absorption rate. For thorium-based cycles, the $\rho_{LZC}(c_{LZC})/\rho^{NU}_{LZC}(c_{LZC})$ ratio rapidly saturates when c_{LZC} increases, indicating that the impact of fuel composition decreases as the LZC becomes more efficient at absorbing neutrons.

4.2. Perturbations sequences

4.2.1. Full core shim mode model

The simplified shim mode model used in St-Aubin and Marleau (2015b) takes into account only in an indirect manner the presence of the LZC in the core. Here, the LZC level variations and ADJ withdrawal, as well as fuel burnup are simulated explicitly using the models developed in Section 3.2. However, the realism of our full core shim mode operation model is limited by the parameterization of the fuel macroscopic cross sections with burnup only. This is insufficient to reflect the effects of the total power variations imposed to the reactor during the shim mode, since as the ADJ banks are extracted from the core, the flux level should increase affecting both the ^{135}I and ^{135}Xe (among other isotopes) concentrations locally. Thus, $\mathscr{P}(t)$ is decreased by operators before adjuster bank withdrawal to avoid spatial power oscillations exceeding the limits. Decreasing $\mathscr{P}(t)$ also extends the shim mode period t^{shim} (in days) when compared to t^{shim}_{∞} (in FPD) defined in St-Aubin and Marleau (2015b). To take into account bulk power variations, the fuel databases should be parameterized minimally with $\mathscr{P}_{cell}$, the power imposed to the fuel cell during the generation of the fuel database in transport, in addition to the burnup (St-Aubin and Marleau, 2015c).

To partially remedy this shortcoming, we impose more and more restrictives zonal power limits as the total reactor power is reduced (similar to Gentilly-2 power station shim operation, see Section 4.3). This does not reflect at all the kinetics effects taking place after a power step back, but has the convenience of allowing higher power peaks in a more accurate core model.

In order to evaluate the core characteristics over the full shim mode period, $t_{n_{max}}$ is set to t_8^-, corresponding to the time when the adjusters driving rule (see Eq. (7)) is met for the 8th times, i.e. when the withdrawal of an additional adjuster rods bank from the core would be required to pursue shim mode operation. Thus, t^{shim} is just the duration of the perturbations sequence $t_{n_{max}}$ in shim mode.

4.2.2. Explicit refueling

LZC optimization during on-power refueling consists first in defining an explicit refueling pattern $\mathscr{E}_j$, describing the refueling order of channel j with an associated refueling frequency $\mathscr{F}_j$. Usually, the parameters $\mathscr{E}_j$, $\mathscr{F}_j$ and the ideal LZC response to the perturbations are determined using coupled neutron diffusion (e.g. DONJON, RFSP) and specialized optimization (e.g. OPTEX, AUTOREFUEL, GENOVA) codes (Rozon et al., 1997; Choi, 2000; Choi and Kim, 2005; Do et al., 2006). In all these optimization codes, the elapsed time between successive refuelings is neglected and this generates symmetrical burnup and power distributions facilitating the LZC responses.

Here, to evaluate the LZC responses in advanced cycles, we do not attempt to optimize the refueling pattern and we do not take directly into account the optimal radial refueling strategy $\overrightarrow{\mathscr{R}}^{\star}$ (see St-Aubin and Marleau (2015a) for the notation used here). Instead, we select *a priori* a single pattern $\mathscr{E}_j$, common to all LZC light water dopings and cycles, combined with time-average refueling frequencies (i.e. $\mathscr{F}_j \approx \overline{\mathscr{F}_j}$), computed explicitly for every cases. This approach is very conservative since in practice operators take great care of optimizing $\mathscr{E}_j$ and $\mathscr{F}_j$. On the other hand, it does not neglect crucial dependencies in the evaluation of the LZC response as some authors have done.

We first assume that $\overrightarrow{\mathscr{R}}^{\star} \approx \vec{1}$ and the time-average power distribution $\overline{\mathscr{P}_z} \approx \overline{\mathscr{P}}^{ref}_z$ in each burnup zone z (defined such that $\overline{\mathscr{F}_j} = \overline{\mathscr{F}_z}, \forall j \in z$). Here, $\overline{\mathscr{P}}^{ref}_z$ is the 3-burnup zone reference cycle time-average power distribution ($\overline{\mathscr{P}}^{ref}_1 = 224.4$ MW, $\overline{\mathscr{P}}^{ref}_2 = 902.1$ MW, $\overline{\mathscr{P}}^{ref}_3 = 937.5$ MW) normalized such that $\overline{\mathscr{P}} = 2064$ MW. This allows to define unique zone power fractions $F_z = \overline{\mathscr{P}}^{ref}_z / \overline{\mathscr{P}}$ for $\mathscr{E}_j$. We then select 28 channels, since this number is a multiple of the number of control zones and produces almost an integer number of channels per burnup

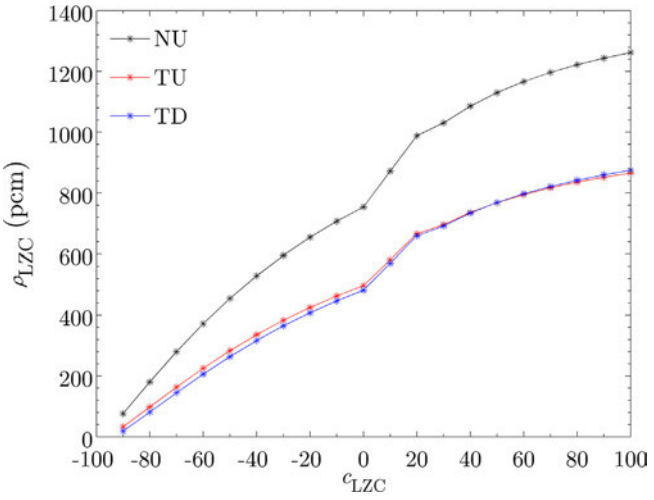

Fig. 4. Variation of ρ_{LZC} with c_{LZC} for NU, TU and TD cycles.

zone ($28F_1 \approx 3$, $28F_2 \approx 12$, $28F_3 \approx 13$). This approach implicitly assumes that all channels of a burnup zone produce the same power. In order to respect the axial and radial refueling symmetries usually followed by operators (Rouben, 1984), 14 channels are selected at both ends of the core in alternance and we choose channels scattered angularly on every radial fuel rings of the core. Our selection of channels also attempts to maximize the LZC levels variations by choosing channels at the limit between two neighboring compartments (see Fig. 2) in order to evaluate the full LZC response potential. The selected refueling pattern is depicted in Fig. 5.

The time-average refueling frequency

$$\overline{\mathscr{F}} = \sum_{z=1}^{3} \overline{\mathscr{F}}_z = \frac{1}{m_{\text{he}} n_s} \sum_{z=1}^{3} \frac{\overline{\mathscr{P}}_z}{\overline{\mathscr{B}}_z^{\text{e}}} \tag{19}$$

used in this model is assessed for every cycles and LZC compositions with the optimal radial refueling strategy $\overrightarrow{\mathscr{R}}^{\star}$ before LZC response simulations using the time-average model presented in St-Aubin and Marleau (2015a). We then assume that $\overline{\mathscr{F}}_j = \overline{\mathscr{F}}$. Here, n_s is the axial refueling strategy that is set to 8 for NU cycle and 4 for TU and TD cycles. With this model, the t_j controlling $\delta\rho_{\text{refuel}}(t)$ defined in Eq. (8) are given by

$$t_j = j\overline{\mathscr{T}}, \tag{20}$$

where $\overline{\mathscr{T}} = 1/\overline{\mathscr{F}}$ is the time-average period. Finally, replacing $t_{r_{\max}}$ by t^{refuel} for the explicit refueling sequence, we set $t^{\text{refuel}} = t_{29}^{-}$, since we choose to refuel 28 channels in this perturbations sequence.

4.3. Optimization constraints and LZC simulation algorithm implementation

With such a broad envelope of core perturbations, a suitable set of optimization constraints must be used in the LZC response and fuel burnup models to respect the modeling assumptions, produce results that can be easily compare with the reference cycles, select efficient LZC levels modification and discard the fuels/LZC compositions mismatches. Here, we provide details about power limits and the actual implementation of the algorithm, while Table 2 presents all the parameters used in the LZC response model.

The power limits $\mathscr{P}_x^{\text{lim}}(t)$ introduced in the spatial iteration (see Section 3.2.2) are given by

$$\mathscr{P}_c^{\text{lim}}(t) = f_c(t)[\mathscr{P}_{c,\text{ref}}^{\text{lim}}(t) + \Delta\mathscr{P}_{c,\text{shape}}^{\text{lim}}], \tag{21}$$

$$\mathscr{P}_{jk}^{\text{lim}}(t) = f_{jk}(t)\mathscr{P}_{jk,\text{ref}}^{\text{lim}}(t), \tag{22}$$

$$\mathscr{P}_{j}^{\text{lim}}(t) = f_{j}(t)\mathscr{P}_{j,\text{ref}}^{\text{lim}}(t), \tag{23}$$

where $\mathscr{P}_{x,\text{ref}}^{\text{lim}}(t)$ are the reference cycle power limits presented in Table 2 for $x = j, jk$, while

$$\mathscr{P}_{c,\text{ref}}^{\text{lim}}(t) = \begin{cases} \overline{\mathscr{P}}_c^{\text{ref}}, & \text{in normal operation} \\ \mathscr{P}_c^{\text{ref}}(t_b^{+}), & \text{if } t_b < t < t_{b+1} \text{ in shim mode} \end{cases}, \tag{24}$$

takes into account the decreasing power steps imposed to the core in shim mode operation (see Section 4.2.1). In Eq. (21), the reference zonal power distribution is corrected with

$$\Delta\mathscr{P}_{c,\text{shape}}^{\text{lim}} = \begin{cases} -12\ \text{MW}, & \text{if } c = 4, 11 \text{ for TD cycle} \\ +2\ \text{MW}, & \text{if } c \neq 4, 11 \text{ for TD cycle} \\ 0\ \text{MW}, & \text{otherwise} \end{cases}, \tag{25}$$

to compensate for the depression observed in the TD cycle channel power distribution (St-Aubin and Marleau, 2015a). The $f_x(t)$ are relaxing factors adjusted with respect to the total reactor power. Those presented in Table 2 are associated with the NU cycle. For TU and TD cycles, $f_{jk}(t) = 1.05$ and $f_j(t) = 1.2$, whereas $f_c(t) = \mathscr{P}_{j,\text{ref}}^{\text{lim}}/\overline{\mathscr{P}}_{j,\text{ref}}^{\text{lim}} = 7300/6700$ for both cycles (St-Aubin and Marleau, 2015a). Tests have been performed using the NU relaxing factors for all cycles, but some of them cannot be controlled adequately, thus we have increased $f_x(t)$ to more appropriate values (St-Aubin, 2013). For shim mode operation, a multiplicative factor

$$\xi_x(t) = \begin{cases} 1.0, & \text{if } t < t_2 \text{ for } x = j, jk \\ 0.9, & \text{if } t_2 \leqslant t < t_5 \text{ for } x = j, jk \\ 0.8, & \text{if } t \geqslant t_5 \text{ for } x = j, jk \\ \mathscr{P}(t)/\overline{\mathscr{P}}, & \text{if } x = c \end{cases} \tag{26}$$

weighting the relaxing factors $f_x(t)$ is used to model the decreasing power ramp.

It is worth noting that Rozon et al. (1997) method did not take into account directly $\mathscr{P}_{jk}^{\text{lim}}(t)$ and $\mathscr{P}_{j}^{\text{lim}}(t)$ limits since this does not reflect the actual RRS control algorithm (Varin et al., 1995), but treating these constraints explicitly avoids diluting them within control zone power limits $\mathscr{P}_{c}^{\text{lim}}(t)$ (Choi, 2000; Choi and Kim, 2005; Do et al., 2006).

Since we do not evaluate *a priori* the effects of the perturbations unlike other authors, some LZC levels might reach 100% while some power constraints are still violated. When this condition arises, we retrieve all the constraints applicable to the compartments when $\mathscr{Y}_c(t) \geqslant 99\%$, because we conclude that the LZC spatial regulation is unable to fulfil its requirements. Even if the saturation of the LZC level might be the result of neglecting the nonlinearity in the LZC response for compartment with $\mathscr{Y}_c(t) \geqslant 80\%$ (see Section 2), taking this effect into account explicitly would not challenge our conclusion on the incapacity of the LZC to manage the power distribution in these cases. Computationally, this constraints relaxation avoids having to perform multiple global-spatial iterations while keeping $\mathscr{Y}_c(t) \in [99, 100]\%$.

It is also important to note that for the shim mode, we do not determine the time t_b at which Eq. (7) is verified, we rather check if $\langle\mathscr{Y}(t)\rangle \leqslant 20\%$ when $\rho(t)$ crosses the lower bound of the detector sensitivity interval at time $t = t_{r+1}^{-}$ before the next ADJ bank withdrawal. This only introduces a very small error since ρ_0 is small (see Table 2) and a numerical uncertainty would be introduced anyway by any algorithm (Brent's method, for instance) trying to solve Eq. (7). Note that if the reactivity cannot be kept within the detector sensitivity interval at this point, it means that the average LZC level $\langle\mathscr{Y}(t)\rangle$ is too low and that an ADJ bank must be extracted to avoid a reactor shutdown. Thus, the algorithm stops.

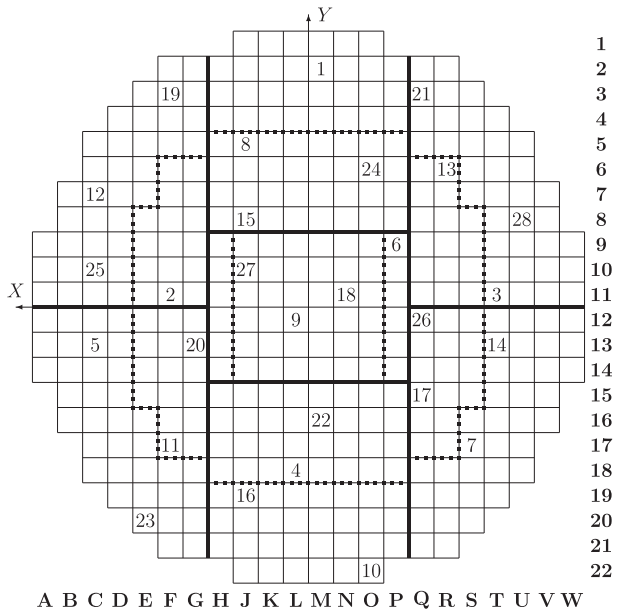

Fig. 5. Explicit refueling pattern $\mathscr{E}_j$ with control (solid) and burnup (dotted) zones limits.

Table 2
Input parameters for the liquid zone controllers response model.

Iteration	Parameter	Value
Global	ρ_0	4 pcm
	ε	1 pcm
	$l^{\max}$	100
Spatial	$\mathscr{P}^{\lim}_{jk,\mathrm{ref}}(t)$	935 kW
	$\mathscr{P}^{\lim}_{j,\mathrm{ref}}(t)$	7 300 kW
	$\mathscr{P}^{\lim}_{c,\mathrm{ref}}(t)$	see Eq. (24)
	$\Delta\mathscr{P}^{\lim}_{c,\mathrm{shape}}$	see Eq. (25)
	$f_c(t)$	1.03
	$f_{jk}(t)$	1
	$f_j(t)$	1
	$\Delta\widetilde{\mathscr{Y}}$	1 %
	$m^{\max}$	200
Global-spatial	$n^{\max}$	100

5. Results and analysis

To evaluate the capacity of the liquid zone controllers to manage the power distribution, relevant metrics coherent with our RRS model must be defined. Since the global iteration stops as soon as $|\rho(t_r^+)| > \rho_0 + \varepsilon$, the global control is ensured if the time t in the simulation reaches $t_{r_{\max}}$ (see Sections 4.2.1 and 4.2.2) before the algorithm stops. Thus, the admissible LZC dopings for a given cycle are first selected using

$$t^{\max} = t_{r_{\max}}, \tag{27}$$

where $t^{\max}$ is the maximal time attained in the simulation. The mean LZC level averaged over time

$$\langle\overline{\mathscr{Y}}\rangle = \frac{1}{t_{r_{\max}}}\int_0^{t_{r_{\max}}}\langle\mathscr{Y}(t)\rangle \mathrm{d}t \tag{28}$$

is a natural metric of the spatial control achieved by the LZC. The distorsions of the LZC responses can also be assessed using the maximal variation of the LZC levels

$$\mathscr{Y}_{\mathrm{amp}}(t) = \max_c \mathscr{Y}_c(t) - \min_c \mathscr{Y}_c(t). \tag{29}$$

It is also crucial to evaluate the effective feedback of the LZC on the power distribution, since some power peaks might exceed the limits. Thus, we define the instantaneous zonal ($x = c$), bundle ($x = jk$) and channel ($x = j$) spatial power control parameters

$$\mathscr{C}_x(t) = 100\% \times \left[\frac{\mathscr{P}^{\max}_x(t) - \mathscr{P}^{\lim}_x(t)}{\mathscr{P}^{\lim}_x(t)}\right] \times \mathscr{H}_x(t), \tag{30}$$

with $\mathscr{P}^{\max}_c(t) = \mathscr{P}_c(t)$ and $\mathscr{H}_x(t)$ is defined in Eq. (16). Averaging $\mathscr{C}_x(t)$ over time, excluding the points t_r, leads to the spatial power control parameter averaged over time:

$$\overline{\mathscr{C}_x} = \frac{1}{t_{r_{\max}}}\left[\int_0^{t_{r_{\max}}}\mathscr{C}_x(t)\mathrm{d}t - \sum_r \int_{t_r^-}^{t_r^+}\mathscr{C}_x(t)\mathrm{d}t\right]. \tag{31}$$

To simplify the analysis, we consider $\overline{\mathscr{C}_c}$ as the components of an Euclidean zonal control vector averaged over time $\overrightarrow{\overline{\mathscr{C}}}$ and define a single metric

$$\|\overrightarrow{\overline{\mathscr{C}}}\| = \sqrt{\sum_{c=1}^{14}\overline{\mathscr{C}_c}^2}. \tag{32}$$

Other relevant metrics have been defined and analyzed in Jeong and Choi (2000) and St-Aubin (2013).

5.1. Reference cycle

Fig. 6 presents (from the bottom to the top) the core reactivity, the LZC average level, the bundle and channel power peaks for the refueling sequence described in Section 4.2.2 for the NU cycle ($t^{\mathrm{refuel}}_{\mathrm{NU}} = 16.26$ FPD). Note that the initial state ($t = 0$) corresponds to the refueled core (state R, see Section 2) with all LZC half-filled ($\delta\rho_{\mathrm{LZC}}(0^-) = 0$ pcm) and all adjusters fully inserted ($\delta\rho_{\mathrm{ADJ}}(0^-) = 0$ pcm). We observe that the reactivity remains in the critical interval except for some points where the instantaneous reactivity variation due to the refueling exceeds the upper bound of the detector sensitivity interval (plus numerical tolerance effects). The detector sensitivity threshold ρ_0 is well-adapted for burnup ($\delta\rho_{\mathrm{burn}}(t)$), since in general the lower bound

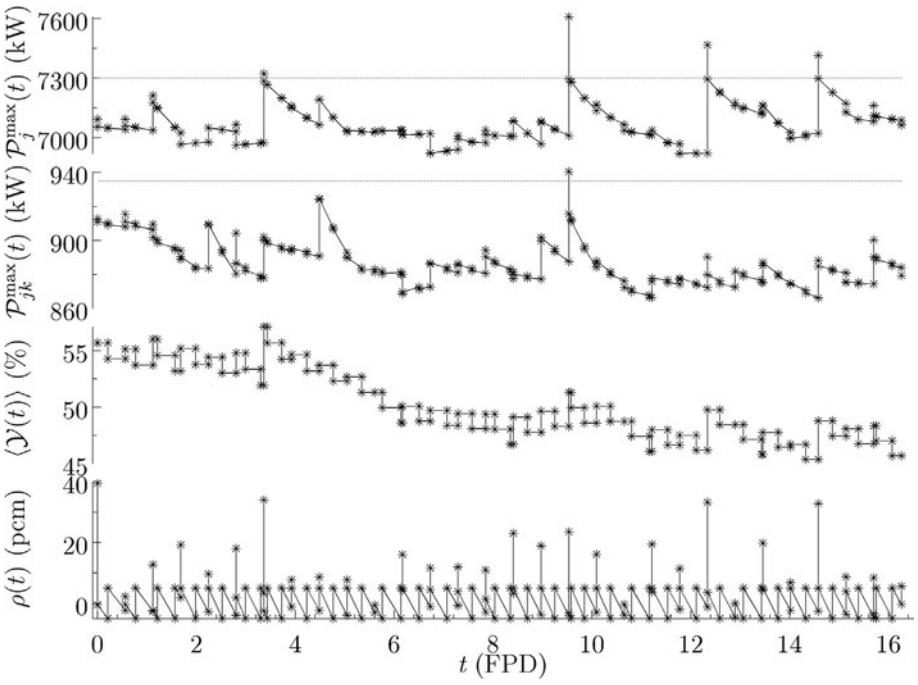

Fig. 6. Variation of the main fuel management and LZC characteristics with full-power time during the explicit refueling period for NU cycle.

$-\rho_0$ is reached at least once between two successive refuelings. This is also true for other LZC dopings and cycles, since $\overline{\mathscr{T}}$ is computed for each case and is directly related to $\partial\delta\rho_{\text{burn}}(t)/\partial t$.

The maximal core reactivity is reached at $t = 0$. A first LZC response ($r = 0$) is performed to cancel the error in the channel age model on the criticality. This results in $\langle\mathscr{Y}(0^+)\rangle = 55.7\%$, $\mathscr{Y}_{\text{amp}}(0^+) = 8.0\%$ and shows that the refueled core with half-filled LZC is slightly supercritical. Taking a closer look at the first refueling ($t_r = 0.56$ FPD), we observe that $\rho(t_r^+) < \rho_0$ indicating that no global iteration were performed, but that spatial iterations were required to decrease some zonal powers, thus decreasing $\rho(t_r^+)$ and increasing $\mathscr{Y}_{\text{amp}}(t_r^+)$ to 19.0%.

Looking at the LZC average level, one sees that it remains between 45.4% and 57.1% during the sequence, which confirms that the MCA remain outside the core (see Section 3.1). This is due to the high accuracy achieved on $\overline{\mathscr{T}}$ and that ρ_0 is small (see Table 2). $\langle\mathscr{Y}(t)\rangle$ tends to decrease with time because our fueling scheme is based on $\overrightarrow{\mathscr{R}}^{\star} \approx \overrightarrow{1}$, while in fact $\mathscr{R}_z^{\star} < 1$ (St-Aubin and Marleau, 2015b). $\mathscr{Y}_{\text{amp}}(t)$ varies only at 3 time points, reaching 22% at the 26th refueling ($t_r = 14.58$ FPD). This does not mean that spatial iterations were only performed 3 times, but that their impact on $\mathscr{Y}_{\text{amp}}(t)$ does not always exceed the amplitude reached before. The lowest and the highest LZC levels recorded during the sequence are respectively 34.0% and 72.6%. The bundle and channel power curves remain below their limits, except once for $\mathscr{P}_{jk}^{\max}(t)$ and 4 times for $\mathscr{P}_j^{\max}(t)$, but the immediate LZC response is appropriate. We conclude that the NU cycle is easy to control, especially since the refueled core state and $\mathscr{E}_j$ have not been optimized.

Fig. 7 presents $\rho(t)$, $\langle\mathscr{Y}(t)\rangle$, $\mathscr{P}_{jk}^{\max}(t)$ and $\mathscr{P}_j^{\max}(t)$ curves for the full core shim mode operation starting at the refueled core state for NU cycle. Since the reactor power is reduced as the time progresses, an effective shim period $t^{\text{shim}} = 56.46$ days that is much greater than $t_{\infty}^{\text{shim}} = 31.86$ FPD is observed. However, taking into account the LZC effects and the decrease in the reactor power, t_{∞}^{shim} over-estimates t^{shim} by 15.3%, because we assumed that $\langle\overline{\mathscr{T}}\rangle = 50\%$ in the simplified model (St-Aubin and Marleau, 2015b), but in fact $\langle\overline{\mathscr{T}}\rangle = 37.2\%$.

The core is perturbed 7 times after the initial state. The amplitudes of these perturbations $\rho_b(t_b)$ are very large and $\rho(t)$ reaches 334 pcm at t_7, which is close to half the delayed neutron fraction for natural uranium β_{NU}. For our thorium-based fuels, $\beta < \beta_{\text{NU}}$ since their ^{233}U and ^{239}Pu contents are higher (Rozon, 1998; St-Aubin and Marleau, 2015) and perturbations of this size may be problematic. In that case, bank 7 could be divided in two sub-banks to avoid such a large reactivity excursion, as was done at the Gentilly-2 power station, the 8th bank being considered in the simulations without additional difficulties. The ADJ bank withdrawal dictates the behavior of $\langle\mathscr{Y}(t)\rangle$ which steps proportionally to ρ_b at times t_b and decreases monotonously until the next bank withdrawal. The period between two successive withdrawals varies between 8.10 FPD (first step) and 3.64 FPD (second step). Even if $\rho_b(t_b)$ increases with b, the individual bank shim period for $b > 2$ remains almost constant when measured in FPD. This has a direct impact on the average rate of decrease of $\langle\mathscr{Y}(t)\rangle$, increasing from 4.5 %/FPD ($t < t_1$) to 8.8 %/FPD ($t > t_7$). $\mathscr{Y}_{\text{amp}}(t)$ varies only for the initial state and after the withdrawal of bank 4. The lowest and highest LZC levels recorded during the shim period are 11.1% at t_7^- and 98.3% at t_7^+, reflecting the bank 7 large reactivity worth. The bundle and channel power peaks jump at t_b and generally decrease between t_b and t_{b+1}, since the higher the local flux level is, the more rapidly the fuel burns. This decreases the amount of fissile isotopes and increases the fission products poisoning, decreasing the local power with time. Slight increases in $\mathscr{P}_j^{\max}(t)$ are observed before t_1 and between t_1 and t_2, because the channel power peak moves in the core. The power steps at t_b are negatives (except for $b = 4$) since the $\mathscr{P}(t)$ is reduced at t_b^-. At t_4, the power distribution shape is strongly perturbed since bank 4 is located on the core middle plane (see Fig. 1) and this is why $\mathscr{P}_{jk}^{\max}(t)$ and $\mathscr{P}_j^{\max}(t)$ increase even if $\mathscr{P}(t)$ decreases.

5.2. Liquid zone controllers doping selection

To select the optimal LZC doping for a given cycle based on both the refueling and shim regimes is not a simple task. However, the latter rarely occurs during the reactor lifetime since qualified teams work daily to maintain the high reliability of the fueling machines and the LZC efficiency is directly related to the ADJ reactivity worth during the shim mode (see Section 5.1). Since ADJ have already been optimized in Part I of this paper and that the impact of the LZC modification on the adjusters is low (as we will show in the following), we neglect the shim mode for the LZC doping selection, although Eq. (27) evaluated with the shim mode is used as a selection criterion to narrow the admissible LZC dopings.

Among the numerous metrics used by Jeong and Choi (2000) and St-Aubin (2013), $\|\overrightarrow{\mathscr{C}}\|$, $\mathscr{C}_{jk}$ and $\mathscr{C}_j$ (see Eqs. (30)–(32)) are the most relevant to LZC fulfilling their requirements during on-power refueling. Since we imposed different power limits for different cycles (see Section 4.3), we define the total spatial control

$$\mathscr{C} = f_c\|\overrightarrow{\mathscr{C}}\| + f_j\mathscr{C}_j + f_{jk}\mathscr{C}_{jk} \tag{33}$$

by penalizing the zone, channel and bundle power control components with their associated power constraint relaxing factor f_x ($f_x(t) = f_x$ during the refueling sequence, see Section 4.3). These penalties do not lead to the same $\mathscr{C}$ that would be obtained if the same f_x were used for all cycles, but they penalize $\mathscr{C}$ in a manner that is coherent with our power limits modeling.

The time-average fuel management advantages or penalties related to doped LZC are considered by the mean of the objective function

$$\Xi(\varepsilon_{\text{axial}}, \overline{\mathscr{P}}_{jk}^{\max}, \overline{\mathscr{P}}_j^{\max}, \langle\overline{\mathscr{B}}^{\text{e}}\rangle) = E(\varepsilon_{\text{axial}}) + P(\overline{\mathscr{P}}_{jk}^{\max}, \overline{\mathscr{P}}_j^{\max}) + B(\langle\overline{\mathscr{B}}^{\text{e}}\rangle), \tag{34}$$

where $E(\varepsilon_{\text{axial}})$ and $P(\overline{\mathscr{P}}_{jk}^{\max}, \overline{\mathscr{P}}_j^{\max})$ are negative step functions that vanish only if their associated constraints (time-average axial convergence, time-average bundle and channel power peaks) are respected at optimal equilibrium. Finally, $B(\langle\overline{\mathscr{B}}^{\text{e}}\rangle) = \langle\overline{\mathscr{B}}^{\text{e}}\rangle/\langle\overline{\mathscr{B}}_{\text{ref}}^{\text{e}}\rangle$, with $\langle\overline{\mathscr{B}}^{\text{e}}\rangle$ the time-average exit burnup averaged over the core. Instantaneous states are also used as selection criteria for admissible LZC dopings (St-Aubin and Marleau, 2015).

Optimal Ξ and $\mathscr{C}$ are respectively associated with their maximal and minimal values, thus we define a global objective function

$$\Theta = \frac{\Xi}{\mathscr{C}} \tag{35}$$

to be maximized. Contrarily to Ξ, Θ does not allow a direct comparison

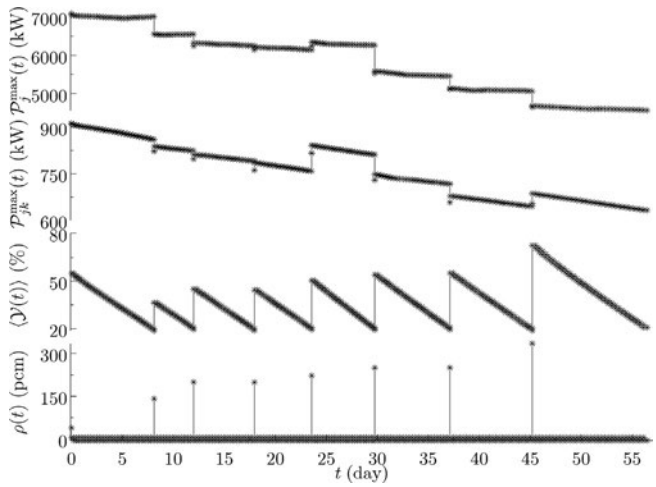

Fig. 7. Variation of the main fuel management and LZC characteristics with time during the shim period for NU cycle.

of the different dopings and cycles. However, the doping associated with the maximal Θ for a given cycle is the best from both the fuel management and spatial control point-of-views. The weighting of Ξ and $\mathscr{C}$ remains arbitrary and could have been determined using other criteria. Here, a decrease of Ξ by a factor of η is justified if $\mathscr{C}$ is also reduced by η. Notice that if Eq. (27) is not respected for one of the perturbations sequence, Θ is not evaluated.

Table 3 presents the first elimination criterion violated for a given c_{LZC} or the value of Θ for the admissible LZC dopings for NU, TU and TD cycles. Ξ, the fresh core (denoted $\mathscr{P}^{\max}_{jk,\mathrm{F}}$ or $\mathscr{P}^{\max}_{j,\mathrm{F}}$) and refueled core (denoted $\mathscr{P}^{\max}_{jk,\mathrm{R}}$ or $\mathscr{P}^{\max}_{j,\mathrm{R}}$) power peaks and the refueling frequency (denoted $\overline{\mathscr{F}}$) conditions defined in St-Aubin and Marleau (2015a) are sequentially assessed before considering adjuster constraints (denoted ρ_{ADJ}) and the shim mode. For shim mode operation, Table 3 presents the first ADJ bank withdrawal for which $\langle \mathscr{Y}(t_b)\rangle = 100\%$, leading to a violation of Eq. (27). For the TU cycle with $c_{\mathrm{LZC}} = -90$, Eq. (27) is violated at $t = 0$ corresponding to state R.

All the cases for which a loss of control during the refueling period have been observed are masked by the criterion on the shim mode due to the intensity of the perturbations. For $c_{\mathrm{LZC}} > 0$, a value of Ξ below 1 is always caused by the P term in Eq. (34) as the E term is never sufficiently penalizing to compensate for the B term when $P = 0$. Except for the TD cycle with $c_{\mathrm{LZC}} = 60$ or 70 for which $\overline{\mathscr{P}}^{\max}_{jk} > \overline{\mathscr{P}}^{\lim}_{jk}$, the time-average channel power constraints are exceeded first. For the reference cycle, $B < 1$ as soon as $c_{\mathrm{LZC}} > 0$, whereas $E = P = 0$. The condition $\Xi \geq 1$ also discriminates the case $c_{\mathrm{LZC}} = -90$ for the TD cycle, for which the time-average channel power peak reaches 898 kW. In this case the channel with peak power is located on a Z-plane ($k = 10$) directly affected by the LZC (see Fig. 1). This indicates that the selected refueling pattern is effectively difficult to control (see Section 4.2.2).

Even if the instantaneous power constraints do not discriminate much dopings, the results for another thorium-based cycle showed that power constraints for the fresh core are systematically exceeded for all LZC dopings considered. This confirms and reinforces the basic analysis presented in St-Aubin and Marleau (2015b) stating that ADJ capacities to flatten the flux distribution can deteriorate when modifying the LZC. For the refueled core, boric acid dopings of LZC decrease greatly the power peaks, making the power limits relaxation of 10% unnecessary for many cases (St-Aubin, 2013).

Only strong heavy water dopings decrease ρ_{ADJ}, the adjuster total reactivity worth, below our objective value $\rho^{\mathrm{obj}}_{\mathrm{ADJ}}$ (St-Aubin and Marleau, 2015b). This is mainly due to the local flux level decrease at the ADJ locations provoked by the radial refueling strategy adjustment for the doped LZC. Indeed, if the LZC absorption rate decreases, the flux level increases at axial core ends and decreases accordingly at the core center. Thus, $\rho_{\mathrm{ADJ}} - \rho^{\mathrm{obj}}_{\mathrm{ADJ}}$, quantifying the LZC-on-ADJ coupling, varies in the ranges [−8, 57] pcm, [16, 111] pcm and [−58, 211] pcm for NU, TU and TD cycles respectively and tends to increase with c_{LZC}. The coarse mesh used during the refueling optimization does not necessarily allow ρ_{ADJ} to increase when ρ_{LZC} increases, but a certain tendency is observed. Eq. (27) is violated only for D_2O-doped LZC since they are then unable to manage the power distribution distortions during the shim period.

In principle, as c_{LZC} increases, $\mathscr{C}$ decreases and Ξ increases, leaving room for an optimum. However, $\Theta(c_{\mathrm{LZC}})$ presents many peaks (except for TD cycle for which $\mathscr{C}(c_{\mathrm{LZC}})$ has a monotone behavior) because of the strong nonlinearity of the LZC response represented here with $\mathscr{C}(c_{\mathrm{LZC}})$ and that $\Xi(c_{\mathrm{LZC}})$ is a uniformly decreasing function. Table 3 reveals that a higher $\langle \overline{\mathscr{B}}^{\mathrm{e}}\rangle$ and a lower $\overline{\mathscr{F}}$ than the reference values can be achieved for the NU cycle with $c_{\mathrm{LZC}} = -10$. Thus, we select respectively 10 v.% D_2O, 1000 ppm H_3BO_3 and 1250 ppm H_3BO_3 dopings for NU, TU and TD cycles.

5.3. Fuel management characteristics with optimal reactivity devices

The optimal reactivity devices being selected for every cycles, the effect of LZC on fuel management and ADJ worth can now be analyzed. The pre-selection of the admissible LZC dopings in agreement with all our selection criteria ensure that these couplings do not challenge any of the conclusions drawn previously. Table 4 presents the main fuel management characteristics in E, F and R states, as well as $\rho_{\uparrow}$, $\rho_{\downarrow}$, ρ_{LZC} and ρ_{ADJ} at optimal equilibrium. Results are presented for the three optimization steps (FUEL, ADJ and LZC) performed. Note that FUEL and ADJ results are equivalent for NU and TU cycles since nominal adjuster rods were selected (St-Aubin and Marleau, 2015a,b).

For all cases, the LZC-on-ADJ coupling remains low, producing changes in ρ_{ADJ} of only 1.1% (NU cycle) to 5.8% (TD cycle). This confirms that our global devices optimization strategy selected in the Part I of this paper is efficient. The main impacts of the LZC on fuel management are respectively 2.5% and 2.3% decreases in $\langle \overline{\mathscr{B}}^{\mathrm{e}}\rangle$ and similar increases in $\overline{\mathscr{F}}$ for TU and TD cycles respectively. Comparing to the nominal devices, $\langle \overline{\mathscr{B}}^{\mathrm{e}}\rangle$ decreases by 7.8% for the TD cycle. Since we selected $c_{\mathrm{LZC}} = -10$ for the NU cycle, $\rho_{\uparrow}$, $\rho_{\downarrow}$, ρ_{LZC} respectively decrease by 5.7%, 6.4% and 6.1%, whereas the maximal poisoning needs ($\delta k^{\mathrm{F}}_{\mathrm{eff}}$) increase by 36 pcm (see definitions of δk_{eff} and NEE in St-Aubin and Marleau (2015a,b)). The channel age model departure from criticality ($\delta k^{\mathrm{R}}_{\mathrm{eff}}$) respectively decreases and increases for H_3BO_3-doped and D_2O-doped LZC. However, a 0.7% increase in $\langle \overline{\mathscr{B}}^{\mathrm{e}}\rangle$ and a 0.6% decrease in $\overline{\mathscr{F}}$ are observed. For TU and TD cycles, the device modifications decrease $\delta k^{\mathrm{F}}_{\mathrm{eff}}$ by 263 pcm and 1501 pcm respectively, including 327 pcm only due to the H_3BO_3-doped LZC for the TD cycle. The fresh core power peaks are still well below the limits for all cases. For the TD cycle, $\mathscr{P}^{\max}_{j,\mathrm{R}}$ increases, whereas $\mathscr{P}^{\max}_{jk,\mathrm{R}}$ is almost constant in spite of the modifications to the reactivity devices. Finally, the increase in $\langle \overline{\mathscr{B}}^{\mathrm{e}}\rangle$ leads to a larger fissile utilization factor (Ξ/NEE) for the NU cycle, whereas the opposite behavior is observed for TU and TD cycles. For all cases, the absolute variations remain below 2.5% and 7.8% when compared with nominal LZC and devices respectively.

6. Conclusions and perspectives

We propose adjustments to the CANDU reactor regulating system in order to improve its control on the power distribution during normal operation for pre-selected thorium-based cycles (St-Aubin and Marleau, 2015a). The goal here is to optimize the liquid zone controllers capacities using innovative modification techniques while maximizing the economical performances of the advanced cycles. Our LZC modification procedure uses a multi-step reactivity devices optimization method in such a way that the pre-selected adjuster rods maintain their minimal

Table 3
Elimination criteria of the LZC dopings and Θ values for admissible dopings for NU, TU and TD cycles.

c_{LZC}	NU	TU	TD
−90	ρ_{ADJ}	State R	Ξ
−80	ρ_{ADJ}	Bank 2	Bank 4
−70	Bank 4	54	$\mathscr{P}^{\max}_{jk,\mathrm{R}}$
−60	Bank 5	63	ρ_{ADJ}
−50	Bank 7	72	ρ_{ADJ}
−40	Bank 7	95	Bank 7
−30	3.7×10^5	102	ρ_{ADJ}
−20	3.3×10^6	105	$\mathscr{P}^{\max}_{j,\mathrm{R}}$
−10	∞	127	499
0	∞	135	593
10	Ξ	144	803
20	Ξ	138	1 723
30	Ξ	141	2 081
40	Ξ	255	3 344
50	Ξ	246	3 356
60	Ξ	246	Ξ
70	Ξ	251	Ξ
80	Ξ	237	Ξ
90	Ξ	Ξ	Ξ
100	Ξ	Ξ	Ξ

Table 4
Main fuel management, ADJ and LZC characteristics at different optimization steps for NU, TU and TD cycles.

Cycle	NU		TU		TD		
Optimization step	FUEL	LZC	FUEL	LZC	FUEL	ADJ	LZC
$\mathscr{R}_2^{\star}$	0.938	0.969	0.969	1.063	0.906	0.938	0.969
$\mathscr{R}_3^{\star}$	0.875	0.906	0.906	0.938	0.875	0.938	0.969
$\overline{\mathscr{P}}_{jk}^{\max}$ (kW)	838	835	818	808	845	843	860
$\overline{\mathscr{P}}_{j}^{\max}$ (kW)	6 685	6 700	6 681	6 633	6 690	6 681	6 686
$\langle\overline{\mathscr{B}}^{e}\rangle$ (GWd/T$_{he}$)	7.254	7.305	32.701	31.880	18.228	17.194	16.804
$\overline{\mathscr{F}}$ (day^{-1})	1.78	1.77	0.85	0.87	1.44	1.53	1.56
Ξ/NEE	1	1.007	1.563	1.524	1.371	1.295	1.264
$\delta k_{\text{eff}}^{\text{F}}$ (pcm)	6 520	6 556	21 161	20 898	23 121	21 947	21 620
$\mathscr{P}_{jk,\text{F}}^{\max}$ (kW)	801	799	807	837	806	754	776
$\mathscr{P}_{j,\text{F}}^{\max}$ (kW)	6 987	6 985	7 043	7 090	7 027	6 577	6 566
$\delta k_{\text{eff}}^{\text{R}}$ (pcm)	39	40	60	56	71	68	57
$\mathscr{P}_{jk,\text{R}}^{\max}$ (kW)	913	908	938	910	993	1 017	1 018
$\mathscr{P}_{j,\text{R}}^{\max}$ (kW)	7 092	7 069	7 355	7 399	7 670	7 908	7 776
ρ_{ADJ} (pcm)	1 694	1 718	1 014	1 042	969	1 886	1 996
$\rho_{\uparrow}$ (pcm)	−332	−313	−221	−317	−311	−208	−319
$\rho_{\downarrow}$ (pcm)	421	394	276	418	396	274	449
ρ_{LZC} (pcm)	753	707	497	735	707	482	768

requirements with the modified LZC.

We developed a novel liquid zone controllers response model based on direct diffusion calculations allowing to control the power distribution during adjuster rods withdrawal and on-power refueling regime. An approach to improve LZC performances using boric acid or heavy water doping is assessed using an objective function taking into account both time-average fuel management and spatial control during pre-determined perturbations sequences. Optimal LZC doping is selected for every cycles in accordance with all the safety, exploitability, economics and adjuster rods requirements. Our analyses show that H_3BO_3 doping enhances spatial control but decreases economics performances, whereas D_2O doping increases the average exit burnup but leads to unmanageable power peaks, especially during adjuster rods withdrawal. The application of our method to the natural uranium cycle demonstrates that both its average exit burnup and refueling frequency can be improved respectively by 0.7% and 0.6% using 10 v.% D_2O-doped LZC, without consequences on the reactor control.

We observed that the selected LZC increase the ADJ total reactivity worth, especially for the TD cycle using ^{113}Cd-doped adjusters. It would be interesting to see if the ADJ doping could be decreased in presence of H_3BO_3-doped LZC, while respecting ADJ minimal requirements. Globally, our fuel and reactivity devices optimization process for advanced cycles allows to find optimal fuel and reactivity management strategies for all kind of nuclear fuels in CANDU reactors.

Acknowledgements

The authors acknowledge the Natural Sciences and Engineering Research Council of Canada, Hydro-Québec and the Organization of CANDU Industries for partly funding this work.

References

Brent, R.P., 1973. Algorithms for Minimization Without Derivatives. Automatic computation. Prentice-Hall Inc., Englewood Cliffs, New Jersey.
Choi, H., 2000. A fast-tunning fuel management program for a CANDU reactor. Ann. Nucl. Energy 27, 1–10.
Choi, H., Kim, D., 2005. Refueling simulation strategy of a CANDU reactor based on optimum zone controller water levels. Nucl. Sci. Eng. 151, 88–94.
Choi, H., Rhee, B., Park, H., 1997. Physics study on direct use of spent pressurized water reactor fuel in CANDU (DUPIC). Nucl. Sci. Eng. 126, 80–93.
Do, Q., Choi, H., Roh, G., 2006. An evolutionary optimization of the refueling simulation for a CANDU reactor. IEEE Trans. Nucl. Sci. 53, 2957–2961.
Harper, B., Gervais, J., Buhl, K., Stone, D., 2012. Boric acid Technical Fact Sheet. Tech. rep. National Pesticide Information Center, Oregon State University Extension Services.
Jeong, C., Choi, H., 2000. Compatibility analysis on existing reactivity devices in CANDU 6 reactors for DUPIC fuel cycle. Nucl. Sci. Eng. 134, 265–280.
Reuss, P., 2003. Précis de neutronique. Génie Atomique, EDP Sciences.
Rouben, B., 1984. Le CANDU – Étude du coeur et gestion du combustible. Tech. Rep. AECL-8333(F). Atomic Energy of Canada Limited, Mississauga, Canada.
Rozon, D., 1998. Introduction to Nuclear Reactor Kinetics. Presses internationales Polytechnique.
Rozon, D., Varin, E., Roy, R., Brissette, D., 1997. Generalized perturbation theory estimates of zone level response to refueling perturbations in a CANDU 600 reactor. In: Advances in Nuclear Fuel Management II. Myrtle Beach, USA.
Shultis, J., Faw, R., 2008. Fundamentals of Nuclear Science and Engineering, 2nd Edition. CRC Press.
St-Aubin, E., 2013. Ajustement du rechargement et des mécanismes de réactivité des réacteurs CANDU pour les cycles de combustible avancés (Ph.D. thesis). École Polytechnique de Montréal, Montréal, Canada.
St-Aubin, E., Marleau, G., 2012. Modeling CANDU-6 liquid zone controllers for effects for thorium-based fuels. In: PHYSOR 2012. Knoxville TN, USA.
St-Aubin, E., Marleau, G., 2015a. CANDU-6 fuel optimization for advanced cycles. Nucl. Eng. Des. 293, 371–384.
St-Aubin, E., Marleau, G., 2015b. CANDU-6 reactivity devices optimization for advanced fuel cycles – Part I: adjuster rods optimization. Nucl. Eng. Des. https://doi.org/10.1016/j.nucengdes.2015.10.027.
St-Aubin, E., Marleau, G., 2015c. Optimized CANDU-6 cell and reactivity device supercell models for advanced fuels reactor database generation. Ann. Nucl. Energy 85, 331–336.
Varin, E., 1995. Intégration des algorithmes du système de régulation du réacteur dans un code de cinétique espace-temps (Master's thesis). École Polytechnique de Montréal, Montréal, Canada.
Varin, E., Koclas, J., Roy, R., 1995. Modeling of the CANDU-6 reactor regulating system. Trans. Am. Nucl. Soc. 73, 428–430.